CORA Cork Open Research Archive
Cartlann Taighde Oscailte Chorcaí

Title	3d absorption-spectra of Sr I through Sr IV
Author(s)	McGuinness, C.; O'Sullivan, G.; Carroll, P. K.; Audley, D.; Mansfield, Michael W. D.
Publication date	1995
Original citation	McGuinness, C., O'Sullivan, G., Carroll, P. K., Audley, D. and Mansfield, M. W. D. (1995) '3d absorption-spectra of Sr I through Sr IV', Physical Review A, 51(3), 2053-2062 (10pp). doi: 10.1103/PhysRevA.51.2053
Type of publication	Article (peer-reviewed)
Link to publisher's version	https://journals.aps.org/pra/abstract/10.1103/PhysRevA.51.2053 http://dx.doi.org/10.1103/PhysRevA.51.2053 Access to the full text of the published version may require a subscription.
Rights	© 1995, American Physical Society
Item downloaded from	http://hdl.handle.net/10468/4564

University College Cork, Ireland
Coláiste na hOllscoile Corcaigh

$3d$ absorption spectra of Sr I through Sr IV

C. McGuinness, G. O'Sullivan, P. K. Carroll, D. Audley,* and M. W. D. Mansfield*

Physics Department, University College Dublin, Belfield, Dublin 4, Ireland

(Received 16 May 1994)

The extreme ultraviolet photoabsorption spectra of neutral to three-times-ionized strontium have been recorded in a comprehensive series of experiments with the dual laser-produced plasma technique. Striking differences were found in the spectra, which can be attributed to the transfer of oscillator strength from $3d \rightarrow np$ to $3d \rightarrow nf$ transitions at Sr^{2+} due to nf wave-function contraction. In Sr and Sr^{+}, $3d \rightarrow 5p$ transitions dominate; in Sr^{2+}, $3d \rightarrow nf$ transitions are most intense, while in Sr^{3+} the $4p$ subshell opens and $3d \rightarrow 4p$ transitions are the strongest features. Partial cross sections for $3d \rightarrow \varepsilon f$ and $3d \rightarrow \varepsilon p$ photoionization were calculated and compared with experiment.

INTRODUCTION

The extreme ultraviolet spectrum of neutral strontium has been extensively analyzed, and discrete features due to $3p$, $3d$, and $4p$ excitation have been identified [1–4]. In these experiments absorption spectra were obtained by backlighting a furnace containing a low pressure of strontium vapor with synchrotron radiation. In subsequent experiments the ratio of double to single photoionization in the 25–36-eV or $4p$ excitation region was measured for neutral strontium [5,6], while the absolute photoionization cross section for Sr^{+} in the 20–41-eV region has been determined by merging beams of monochromatic synchrotron radiation and unexcited Sr^{+} ions [7] and the results compared with electron impact ionization data [8]. Apart from a report of an unassigned spectrum which contained lines due to both Sr and Sr^{+} [9], no data exist for $3d$ photoionization in low ion stages of ionized strontium. This lack of data stems from the difficulty in simultaneously obtaining an ion density of sufficient magnitude and combining it with a suitable XUV continuum source.

A recent development has been the successful crossing of ion beams from an ECR (electron cyclotron resonance) source with synchrotron radiation, which facilitated an extensive photoionization study and analysis of the spectrum of Ca^{+} [10,11]. Using photoelectron detection, absolute cross sections were determined, but because of the low photoelectron flux experimental resolution was restricted to ± 0.2 eV, which is adequate for continua or broad features but can present difficulties in interpreting spectra from regions with a high density of sharp discrete features. An alternative method for exploring inner shell spectra which gives good energy resolution but at best only relative cross sections is the dual laser-produced plasma technique [12–14], which has been successfully

employed to study trends along extended isoelectronic sequences and to obtain subvalence spectra from refractory elements [15,16]. In this technique a plasma of the species of interest is first generated by focusing the output of a high power pulsed laser onto a suitable slab target and then after a fixed time delay τ backlighting it with a transient XUV continuum pulse from a second laser-produced plasma. A comprehensive survey of the emission spectra of Q-spoiled laser-produced plasmas has shown that elements with $62 \leq Z \leq 74$ provide line free continuum emission over extensive energy ranges and in particular that the spectrum of samarium ($Z = 62$) is essentially line free from 6 to 400 eV [17]. Ion stage "tuning" in the absorbing plasma can be obtained either by varying τ or the incident laser pulse power density ϕ which can be changed by reducing the incident pulse energy or altering the focusing conditions at the target. In practice, simple calculations based on models of laser-produced plasmas such as the collisional radiative (CR) model of Colombant and Tonon [18] make it possible to set the experimental conditions under which ion stage separation is optimized.

EXPERIMENT

In the present case a 1.5-J, 30-ns ruby laser pulse was focused onto a strontium target via a planoconvex, cylindrical lens assembly which gave plasma lengths l of 2, 6, or 12 mm and widths of 0.2 mm. An 860-mJ, 10-ns pulse from a Nd:YAG (neodymium:yttrium aluminum garnet) oscillator-amplifier assembly focused onto a samarium target to a power density of 4.6×10^{11} W cm^{-2} generated the background continuum. Spectra were recorded photographically on a 2-m grazing incidence vacuum spectrograph in which the dispersion varied from 0.4 eV mm^{-1} at 75 eV to 1.2 eV mm^{-1} at 150 eV. Insertion of a variable time delay between the Pockels cell control pulses enabled τ to be varied. Since typically 500 shots are required to produce a spectrum, τ was monitored for each shot and a mean value jitter obtained for each run. The shot-to-shot reproducibility was within ± 10 ns in each case. Wavelength measurements were performed

————————

*Also at Physics Department, University College Cork, Cork, Ireland.

    <u>51</u>   2053

TABLE I. Energies of transitions observed in strontium laser-produced plasmas.

Plasma Conditions:	Laser Time Delay:	Power Density:	Ions Present:
6 mm	251 ns	2.8×10^9 W cm^{-2}	60% Sr II, 40% Sr I
2 mm	197 ns	9.0×10^9 W cm^{-2}	80% Sr II, 20% Sr I
6 mm	82 ns	2.8×10^9 W cm^{-2}	5% Sr I, 80% Sr II, 15% Sr III
2 mm	63 ns	9.0×10^9 W cm^{-2}	40% Sr II, 60% Sr III
2 mm	60 ns	1.1×10^{10} W cm^{-2}	25% Sr II, 65% Sr III, 10% Sr IV

Energies Observed (eV)				6 mm / 251 ns	2 mm / 197 ns	6 mm / 82 ns	2 mm / 63 ns	2 mm / 60 ns
Sr I	Sr II	Sr III	Sr IV					
			115.08					Clear
			115.64					Clear
			116.76					Clear
137.36				Clear	Very faint, imprecise			
	137.91			Faint	Clear but asymmetric	Clear but asymmetric	Clear but asymmetric	
	139.45					139.36		
	139.61			Very broad feature	Very broad feature	139.56 Broadened	Very broad feature	
	139.75					139.75		
		141.08				Broadened	Clear	
		141.31				Broadened	Clear	
	141.78			Clear	Clear	Faint		
	142.12			Clear	Clear	Faint		
		142.90				Clear	Definite	Definite
	143.78				Very Faint	Faint		
	143.92							
		144.48				Clear	Definite	Definite
	144.52					Faint		
	145.20			Clear	Definite	Definite		
	146.90			Clear	Definite	Definite		
		149.83				Faint hint	Very clear	Very clear
		151.61				Faint hint	Very clear	Very clear
		152.78					Very clear	Very clear
		154.38					Clear, but also broader	Clear, but also broader
		156.15					Imprecise	Imprecise

using a photoelectric comparator or directly from photographic enlargements. Wavelength calibration was obtained by superimposing spectra of Al IV through Al IX from laser-produced aluminum plasmas [19]. The accuracy of wavelength determination was estimated by calculating the residuals from a cubic polynomial when fitted to the Al reference lines. The maximum absolute value of a residual was always below 0.015 eV, while the standard deviation of the residuals was always below 0.009 eV. When allowance is made for the broad nature of the absorption lines, the measurement accuracy is estimated at ± 0.02 eV.

RESULTS

The energies of the principal features obtained as well as the experimental conditions (τ, l, ϕ) under which they were observed are listed in Table I. At $\tau = 251$ ns, the Sr I resonance $3d^{10}4s^{2}4p^{6}5s^{2}\,^{1}S_{0} \rightarrow 3d^{9}4s^{2}4p^{6}5s^{2}5p\,^{1}P_{1}$ transition at 137.36 eV is clearly visible. For an increase in ϕ of 50% and a decrease in τ to 197 ns, the spectrum of Sr^{+} becomes stronger. At $\tau = 82$ ns the spectrum is predominantly Sr^{+} and Sr^{2+}, while at $\tau = 60$ ns for $\phi = 1.1 \times 10^{10}$ W cm^{-2} the spectrum contains only Sr^{2+} and Sr^{3+}. In order to identify the transitions, *ab initio* atomic structure calculations were performed using the HXR computer codes of Cowan [20].

After each spectrum was recorded, measurements were made of the typical laser crater size on the strontium target, and the mean laser power density ϕ was calculated. Using the equation for irradiation at a laser wavelength λ,

$$T_{e} = 5.2 \times 10^{-6} Z^{1/5} (\lambda^{2}\phi)^{3/5} ,$$

from Ref. [18] the electron temperature T_{e} of the strontium plasma during the laser pulse was deduced. In the steady-state collisional-radiative ionization model of Ref. [18], the ratio of number density of ion state $Z + 1$ to ion state Z is given by

$$\frac{N_{z+1}}{N_{z}} = S(Z, T_{e})[\alpha_{r}(Z+1, T_{e}) + n_{e}\alpha_{3b}(Z+1, T_{e})]^{-1} ,$$

where $S(Z, T_{e})$, $\alpha_{r}(Z, T_{e})$, and $\alpha_{3b}(Z, T_{e})$ are the collisional ionization, radiative recombination, and three-body recombination coefficients of an ion of charge Z at temperature T_{e}; N_{e} was chosen to correspond to the cutoff density for 694-nm radiation. From this equation it was possible to compute the ratio $N_{z}|\sum_{k=1}^{z}N_{k}$, the fractional number density of charge Z, and plot its evolution as a function of T_{e} as in Fig. 1, where the electron temperatures of three typical absorbing plasmas are indicated. It should be noted that this corresponds to a steady-state distribution achieved during the laser pulse. After this time the plasma expands, cools, and recombines, and the average charge state decreases. Furthermore this estimation of charge state distribution within the plasma is confirmed by the absorption spectra which are recorded. In each case the maximum charge state observed is that predicted by the model, while the ratios of charge state $Z + 1$ to charge state Z are lower than pre-
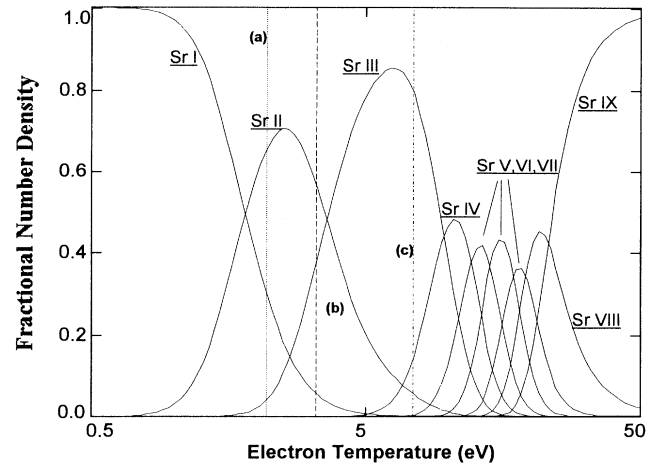

FIG. 1. Fractional number densities of the charge states of strontium plotted with increasing electron temperature on a logarithmic scale. The three bars indicated are the electron temperatures corresponding to the three typical plasma columns created in the experiment: (a) 12-mm plasma length, (b) 6-mm plasma length, and (c) 2-mm plasma length.

dicted because of the effects of recombination at longer-time delays.

THE 3d SPECTRUM OF NEUTRAL Sr

The 3d subvalence spectrum of Sr I was photographed in experiments using synchrotron radiation and windowless furnaces, and the analysis allowed for strong $5s, 4d$ mixing effects [1,2]. A comparison between the 3d spectra of Rb I and Sr I [3] showed that in Rb I there is both $3d^{9}5s5p$ term dependence which causes a departure of the $(5s5p\,^{1}P)$-based term energies from their configuration average values and $3d^{9}5s5p$ and $3d^{9}4d5p$ mixing which results in a depression of the energies of the $3d^{9}(5s5p\,^{1}P)$-based levels and a reduction in the single configuration purity of these levels to between 61 and 78%. The $3d^{9}(5s5p\,^{3}P)$-based levels and higher-energy $3d^{9}5snp$ configurations are relatively unaffected, so that well-developed Rydberg series are obtained. In contrast, in Sr I, interaction between the different levels of the $3d^{9}(5s^{2}+4d5s+4d^{2})np$ ($n = 5$ and 6) complex produces a large number of intense lines in the region where Rydberg structure is expected. The increased strength of configuration interaction in Sr I arises because the 4d wave function is beginning to collapse into the core producing a large $4d, 5s$ overlap.

In the present case the first two members of the Sr I spectrum were observed in the spectra recorded at $\tau = 251$ and 197 ns. The peak center of the lowest-energy transition appears to be at 92.26 Å. The earlier HXR calculations performed with the Cowan code [20] were repeated. The F^{k}, G^{k}, and R^{k} integrals were reduced by 10%. Reductions in the range 5–20 % are required to allow for configuration-interaction effects not included explicitly in the calculation [20]. In the present case a 10% reduction was found to give the best estimate of the energy separations of the individual lines, and allowed them

to be fitted to the experimental data with an energy shift which was the same for all transitions. The results of these calculations are presented graphically in Fig. 2(a), where a constant shift of -0.08 eV seems to optimize agreement between prediction and observation, at least for the features observed here. In obtaining the theoretical spectrum each transition was given an intensity proportional to its oscillator strength (gf value), and an artificial Gaussian linewidth of 0.10 eV which was found to give optimum agreement with the experimental data. This width compares favorably with the calculated Auger $3d$ widths for Kr I of 0.089 eV [21] and Rb I of 0.079 eV [22], as the $3d$ hole in neutral strontium is known to decay preferentially by similar Auger processes to Sr^{3+} [23]. Because of the possibility of saturation of the photographic emulsion in addition to the fact that the majority of the observed features are blends of more than one transition, no detailed attempt was made to extract linewidths in the present case. However, the overall agreement between the theoretical and experimental line

profiles especially within a given ion stage would seem to indicate that the photographic response was essentially linear under the conditions described here. The spectrum contains both neutral Sr and Sr^+, and a population mixture of 60% Sr and 40% Sr^+ was chosen in constructing the theoretical fit as it seemed to give near-optimum agreement with experiment. The calculations showed that $3d \rightarrow nf$ transitions had vanishing oscillator strength due to the centrifugal repulsion of nf electrons from the core region.

THE $3d$ SPECTRUM OF Sr^+

In Sr^+ the effects of $4d$ collapse are expected to be even more significant, and while the ground configuration is $3d^{10}5s$, the $3d^{10}4d_{3/2}$ and $3d^{10}4d_{5/2}$ levels are only 1.8046 and 1.8393 eV away [24]. Moreover the center of gravity of the excited $3d^9 5s 5p$ configuration is predicted by the present calculations to lie above the $3d^9 4d 5p$ by
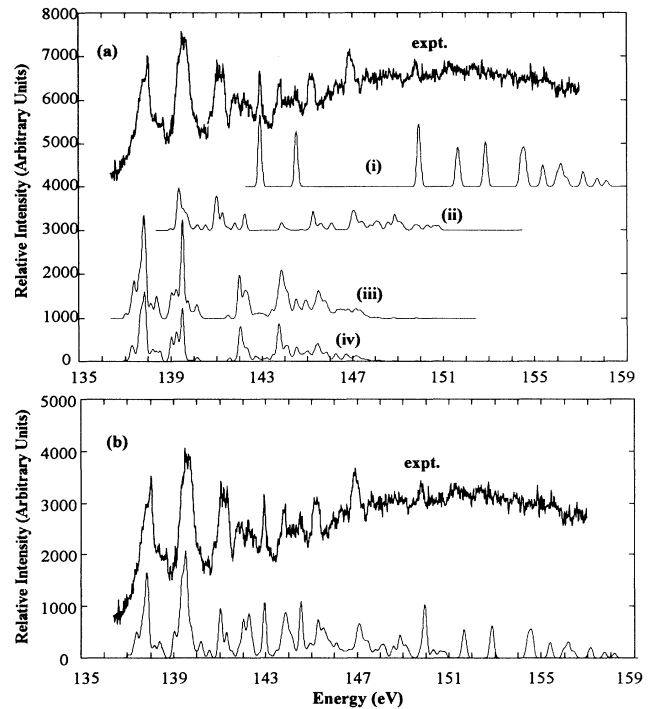

FIG. 2. Plot of the microdensitometer trace of the absorption of a strontium laser-produced plasma of column length 2 mm, taken at an interplasma time delay of 197 ns. Part (a) shows the trace and the following theoretical spectra: (i) Sr I $3d^{10}4s^24p^65s^2 \rightarrow 3d^94s^24p^65s^2[np,mf]$, (ii) Sr II $3d^{10}4s^24p^65s \rightarrow 3d^94s^24p^6[5s+4d][np,mf]$, (iii) Sr II $3d^{10}4s^24p^64d$ $(j=\frac{5}{2}) \rightarrow 3d^94s^24p^6[4d+5s][np,mf]$, and (iv) Sr II $3d^{10}4s^24p^64d(j=\frac{3}{2}) \rightarrow 3d^94s^24p^6[4d+5s][np,mf]$, which were shifted by the following amounts: -0.08, $+0.65$, $+0.4$, and $+0.4$ eV, respectively, to fit the observed data. In all of the above n ranged form 5 to 11 and m ranged from 4 to 9. Part (b) shows a combined plot of these theoretical spectra in the ratios 20:56:14:10, respectively, and compared to the observed absorption. All of the spectral lines in the theoretical plots have been given a Gaussian width of 0.1 eV.

FIG. 3. Plot of the microdensitometer trace of the absorption of a strontium-laser-produced plasma of column length 6 mm, taken at an interplasma time delay of 82 ns. Part (a) shows the trace and the following theoretical spectra: (i) Sr III $3d^{10}4s^24p^6 \rightarrow 3d^94s^24p^6[np,mf]$, (ii) Sr II $3d^{10}4s^24p^65s \rightarrow 3d^94s^24p^6[5s+4d][np,mf]$, (iii) Sr II $3d^{10}4s^24p^64d(j=\frac{5}{2}) \rightarrow 3d^94s^24p^6[4d+5s][np,mf]$, and (iv) Sr II $3d^{10}4s^24p^64d$ $(j=\frac{3}{2}) \rightarrow 3d^94s^24p^6[4d+5s][np,mf]$, which were shifted by the following amounts: $+0.55$, $+0.65$, $+0.4$, and $+0.4$ eV, respectively, to fit the observed data. In all of the above n ranged from 5 to 11 and m ranged from 4 to 9. Part (b) shows a combined plot of these theoretical spectra in the ratios 24:46:18:12, respectively, and compared with the observed absorption. All of the spectral lines in the theoretical plots have been given a Gaussian width of 0.1 eV.

TABLE II. The 3d photoabsorption spectrum of Sr II. Only the transitions whose calculated gf value is above 0.0020 are included in this table. This is only 44 lines out of 3038. The experimental values are taken from Table I, but consultation of Figs. 2–5 is advisable. The calculated values for the energies are given prior to shifting to match the experimental data. Shifts of 0.65 eV were used for transitions whose lower level is $3d^9 4s^2 4p^6 5s 5p$, while 0.40 eV was used for transitions whose lower level was $3d^9 4s^2 4p^6 4d 5p$. Also, the LS composition of each level is given in terms of the leading LS term and then the summation of the larger contributions to each level according to configurations; all contributions less than 10% are classified as other.

		E (ev)				
Lower level	Upper level	Expt.	Calc.	gf value	$J \rightarrow J$	LS composition
$3d^{10} 4s^2 4p^6 5s$	$3d^9 4s^2 4p^6 5s 5p$	139.61	138.6597	0.0046	$\frac{1}{2} \rightarrow \frac{3}{2}$	$19\%(^3D)^4P + 27\%3d^9 4s^2 4p^6 5s 5p + 25\%3d^9 4s^2 4p^6 4d 5p + 29\%$ other
	$3d^9 4s^2 4p^6 5s 5p$		138.7104	0.0055	$\frac{1}{2} \rightarrow \frac{1}{2}$	$32\%(^1D)^2P + 29\%3d^9 4s^2 4p^6 4d 5p + 10\%3d^9 4s^2 4p^6 5s 5p + 29\%$ other
	$3d^9 4s^2 4p^6 4d 5p$		139.0538	0.0025	$\frac{1}{2} \rightarrow \frac{3}{2}$	$16\%(^3P)^2P + 39\%3d^9 4s^2 4p^6 4d 5p + 45\%$ other
	$3d^9 4s^2 4p^6 5s 5p$	141.08	140.3041	0.0032	$\frac{1}{2} \rightarrow \frac{3}{2}$	$15\%(^3D)^4P + 39\%3d^9 4s^2 4p^6 4d 5p + 46\%$ other
	$3d^9 4s^2 4p^6 4d 5p$		140.3877	0.0036	$\frac{1}{2} \rightarrow \frac{3}{2}$	$18\%(^1P)^2D + 28\%3d^9 4s^2 4p^6 4d 5p + 56\%$ other
	$3d^9 4s^2 4p^6 4d 5p$	141.31	140.6101	0.0033	$\frac{1}{2} \rightarrow \frac{3}{2}$	$15\%(^3P)^4S + 14\%3d^9 4s^2 4p^6 5s 5p + 14\%3d^9 4s^2 4p^6 4d 5p + 57\%$ other
	$3d^9 4s^2 4p^6 5s 5p$	142.12	141.5954	0.0037	$\frac{1}{2} \rightarrow \frac{3}{2}$	$45\%(^3D)^2P + 13\%3d^9 4s^2 4p^6 5s 5p + 42\%$ other
	$3d^9 4s^2 4p^6 5s 6p$	145.20	144.6060	0.0021	$\frac{1}{2} \rightarrow \frac{3}{2}$	$32\%(^3D)^4P + 43\%3d^9 4s^2 4p^6 5s 6p + 25\%$ other
$3d^{10} 4s^2 4p^6 4d$	$3d^9 4s^2 4p^6 5s 5p$		136.8688	0.0025	$\frac{3}{2} \rightarrow \frac{5}{2}$	$25\%(^1D)^2F + 20\%3d^9 4s^2 4p^6 5s 5p + 55\%$ other
	$3d^9 4s^2 4p^6 4d 5p$		136.9736	0.0069	$\frac{5}{2} \rightarrow \frac{7}{2}$	$42\%(^3G)^2F + 22\%3d^9 4s^2 4p^6 4d 5p + 36\%$ other
	$3d^9 4s^2 4p^6 4d 5p$		137.1912	0.0027	$\frac{5}{2} \rightarrow \frac{3}{2}$	$35\%(^3D)^2P + 10\%3d^9 4s^2 4p^6 4d 5p + 55\%$ other
	$3d^9 4s^2 4p^6 4d 5p$		137.2066	0.0030	$\frac{5}{2} \rightarrow \frac{7}{2}$	$21\%(^3D)^2F + 28\%3d^9 4s^2 4p^6 4d 5p + 13\%3d^9 4s^2 4p^6 5s 5p + 38\%$ other
	$3d^9 4s^2 4p^6 4d 5p$		137.2202	0.0047	$\frac{3}{2} \rightarrow \frac{1}{2}$	$17\%(^3D)^4D + 39\%3d^9 4s^2 4p^6 4d 5p + 10\%3d^9 4s^2 4p^6 5s 5p + 34\%$ other
	$3d^9 4s^2 4p^6 4d 5p$		137.2647	0.0026	$\frac{5}{2} \rightarrow \frac{3}{2}$	$16\%(^3P)^2P + 39\%3d^9 4s^2 4p^6 4d 5p + 45\%$ other
	$3d^9 4s^2 4p^6 4d 5p$		137.2863	0.0023	$\frac{5}{2} \rightarrow \frac{7}{2}$	$26\%(^3F)^4F + 32\%3d^9 4s^2 4p^6 4d 5p + 42\%$ other
	$3d^9 4s^2 4p^6 4d 5p$		137.3253	0.0084	$\frac{3}{2} \rightarrow \frac{5}{2}$	$17\%(^1F)^2F + 48\%3d^9 4s^2 4p^6 4d 5p + 35\%$ other
	$3d^9 4s^2 4p^6 4d 5p$	137.91	137.3764	0.0082	$\frac{5}{2} \rightarrow \frac{7}{2}$	$21\%(^3D)^4D + 35\%3d^9 4s^2 4p^6 4d 5p + 44\%$ other
	$3d^9 4s^2 4p^6 4d 5p$		137.3988	0.0034	$\frac{5}{2} \rightarrow \frac{5}{2}$	$20\%(^1F)^2D + 22\%3d^9 4s^2 4p^6 4d 5p + 56\%$ other
	$3d^9 4s^2 4p^6 4d 5p$		137.4126	0.0034	$\frac{5}{2} \rightarrow \frac{7}{2}$	$30\%(^1D)^2F + 30\%3d^9 4s^2 4p^6 4d 5p + 40\%$ other
	$3d^9 4s^2 4p^6 4d 5p$		137.4198	0.0025	$\frac{5}{2} \rightarrow \frac{3}{2}$	$19\%(^1D)^2D + 44\%3d^9 4s^2 4p^6 4d 5p + 37\%$ other
	$3d^9 4s^2 4p^6 4d 5p$		137.4393	0.0059	$\frac{3}{2} \rightarrow \frac{5}{2}$	$20\%(^1F)^2D + 23\%3d^9 4s^2 4p^6 4d 5p + 57\%$ other
	$3d^9 4s^2 4p^6 4d 5p$		137.4603	0.0082	$\frac{3}{2} \rightarrow \frac{3}{2}$	$19\%(^1D)^2D + 45\%3d^9 4s^2 4p^6 4d 5p + 36\%$ other
	$3d^9 4s^2 4p^6 4d 5p$		137.4679	0.0096	$\frac{5}{2} \rightarrow \frac{5}{2}$	$27\%(^3F)^2D + 18\%3d^9 4s^2 4p^6 4d 5p + 55\%$ other
	$3d^9 4s^2 4p^6 4d 5p$		137.7264	0.0025	$\frac{5}{2} \rightarrow \frac{3}{2}$	$16\%(^3D)^4P + 25\%3d^9 4s^2 4p^6 4d 5p + 59\%$ other
	$3d^9 4s^2 4p^6 4d 5p$		137.9663	0.0028	$\frac{5}{2} \rightarrow \frac{5}{2}$	$17\%(^3F)^4D + 26\%3d^9 4s^2 4p^6 4d 5p + 57\%$ other
	$3d^9 4s^2 4p^6 5s 5p$		138.6039	0.0029	$\frac{3}{2} \rightarrow \frac{5}{2}$	$45\%(^3D)^4F + 14\%3d^9 4s^2 4p^6 5s 5p + 13\%3d^9 4s^2 4p^6 4d 5p + 28\%$ other
	$3d^9 4s^2 4p^6 5s 5p$		138.6518	0.0024	$\frac{5}{2} \rightarrow \frac{7}{2}$	$26\%(^1D)^2F + 23\%3d^9 4s^2 4p^6 5s 5p + 12\%\ 3d^9 4s^2 4p^6 4d 5p + 39\%$ other
	$3d^9 4s^2 4p^6 4d 5p$		138.8027	0.0044	$\frac{3}{2} \rightarrow \frac{5}{2}$	$30\%(^3G)^2F + 12\%3d^9 4s^2 4p^6 4d 5p + 58\%$ other
	$3d^9 4s^2 4p^6 4d 5p$		138.8210	0.0035	$\frac{5}{2} \rightarrow \frac{3}{2}$	$15\%(^3P)^4S + 14\%3d^9 4s^2 4p^6 4d 5p + 14\%3d^9 4s^2 4p^6 5s 5p + 57\%$ other
	$3d^9 4s^2 4p^6 4d 5p$		138.8929	0.0022	$\frac{5}{2} \rightarrow \frac{7}{2}$	$55\%(^3G)^4G + 26\%3d^9 4s^2 4p^6 4d 5p + 19\%$ other
	$3d^9 4s^2 4p^6 4d 5p$		139.0425	0.0034	$\frac{5}{2} \rightarrow \frac{7}{2}$	$25\%(^3D)^4F + 42\%3d^9 4s^2 4p^6 4d 5p + 23\%$ other
	$3d^9 4s^2 4p^6 4d 5p$		139.0800	0.0059	$\frac{3}{2} \rightarrow \frac{3}{2}$	$11\%(^3D)^4D + 21\%3d^9 4s^2 4p^6 4d 5p + 68\%$ other
	$3d^9 4s^2 4p^6 4d 5p$	139.61	139.0862	0.0091	$\frac{5}{2} \rightarrow \frac{5}{2}$	$17\%(^1D)^2D + 29\%3d^9 4s^2 4p^6 4d 5p + 54\%$ other
	$3d^9 4s^2 4p^6 4d 5p$		139.1084	0.0026	$\frac{3}{2} \rightarrow \frac{5}{2}$	$18\%(^3F)^4F + 31\%3d^9 4s^2 4p^6 4d 5p + 51\%$ other
	$3d^9 4s^2 4p^6 4d 5p$		139.1181	0.0101	$\frac{5}{2} \rightarrow \frac{7}{2}$	$15\%(^1F)^2F + 23\%3d^9 4s^2 4p^6 4d 5p + 62\%$ other
	$3d^9 4s^2 4p^6 4d 5p$		139.1268	0.0023	$\frac{3}{2} \rightarrow \frac{5}{2}$	$17\%(^1D)^2D + 29\%3d^9 4s^2 4p^6 4d 5p + 54\%$ other
	$3d^9 4s^2 4p^6 4d 5p$		139.3393	0.0034	$\frac{5}{2} \rightarrow \frac{3}{2}$	$29\%(^3D)^2D + 31\%3d^9 4s^2 4p^6 4d 5p + 40\%$ other
	$3d^9 4s^2 4p^6 4d 5p$		139.7295	0.0024	$\frac{5}{2} \rightarrow \frac{5}{2}$	$22\%(^3D)^2F + 44\%3d^9 4s^2 4p^6 4d 5p + 34\%$ other
	$3d^9 4s^2 4p^6 4d 6p$	141.78	141.5907	0.0020	$\frac{5}{2} \rightarrow \frac{3}{2}$	$35\%(^1D)^2P + 21\%3d^9 4s^2 4p^6 4d 6p + 44\%$ other
	$3d^9 4s^2 4p^6 4d 6p$		141.5985	0.0065	$\frac{5}{2} \rightarrow \frac{7}{2}$	$58\%(^3G)^2F + 14\%3d^9 4s^2 4p^6 4d 6p + 28\%$ other

TABLE II. *(Continued)*.

Lower level	Upper level	E (ev) Expt.	Calc.	gf value	$J \to J$	LS composition
	$3d^94s^24p^65s6p$	142.12	141.6283	0.0036	$\frac{3}{2} \to \frac{5}{2}$	$17\%(^3D)^2F + 35\%3d^94s^24p^65s6p + 51\%$ other
$3d^94s^24p^64d6p$			141.8170	0.0022	$\frac{5}{2} \to \frac{5}{2}$	$29\%(^3D)^2D + 71\%$ other
$3d^94s^24p^64d6p$		143.78	143.3307	0.0022	$\frac{5}{2} \to \frac{7}{2}$	$29\%(^1G)^2G + 23\%3d^94s^24p^64d6p + 10\%3d^94s^24p^64d7p + 38\%$ other
$3d^94s^24p^64d7p$			143.4209	0.0022	$\frac{5}{2} \to \frac{7}{2}$	$19\%(^3D)^4D + 23\%3d^94s^24p^64d6p + 23\%3d^94s^24p^64d7p + 35\%$ other

0.107 eV. This has two effects on the spectrum; first, there is strong configuration mixing between $3d^95snp$ and $3d^94dnp$ levels; and second, because of the proximity of the metastable $3d^{10}4d$ terms to the ground state the spectrum is expected to contain a significant contribution from excited state absorption, especially since as implied in Fig. 1, an electron temperature of the order of approximately 1 eV is required to observe Sr^+ in an equilibrium plasma.

HXR calculations were performed for the following sets of transitions:

$$3d^{10}5s \to 3d^9(5s + 4d)np, mf, \quad 5 \le n \le 11, \quad 4 \le m \le 9,$$

$$3d^{10}4d(j = \tfrac{3}{2}) \to 3d^9(5s + 4d)np, mf,$$

$$5 \le n \le 11, \quad 4 \le m \le 9,$$

$$3d^{10}4d(j = \tfrac{5}{2}) - 3d^9(5s + 4d)np, mf,$$

$$5 \le n \le 11, \quad 4 \le m \le 9.$$

From these, synthetic spectra were constructed as before and compared with the experimental data (Figs. 2 and 3). It is seen from these figures that a systematic shift of 0.65 eV toward higher energy for the $3d^{10}5s$ excitation spectrum and 0.40 eV toward higher energy for the $3d^{10}4d$ spectrum gives the best agreement between theory and observation, especially for the lowest series members. Again, in these calculations, the F^k, G^k, and R^k integrals were reduced by 10%. In Fig. 3(a) the results of the individual calculations above are shown, while in Fig. 3(b) they are compared in the ratio $60\%3d^{10}5s + 16\%3d^{10}4d(j = \tfrac{3}{2}) + 26\%3d^{10}4d(j = \tfrac{5}{2})$ with the ex-

TABLE III. The $3d$ photoabsorption spectrum of Sr II. Lower level : $3d^{10}4s^24p^6$.

Upper level:	E (ev) Expt.	Calc.	gf value:	$J \to J$	LS composition:	jj composition
$3d^94s^24p^65p$	142.90	142.369	0.0166	$0 \to 1$	$56\%(^2D)^1P, 35\%(^2D)^3P, \underline{9\%}(^2D)^3D$	$100\%(\tfrac{3}{2},\tfrac{3}{2})$
	144.48	143.969	0.0130	$0 \to 1$	$49\%(^2D)^3P, \underline{44\%}(^2D)^1P, \underline{8\%}(^2D)^3D$	$\underline{74\%}(\tfrac{3}{2},\tfrac{1}{2}), 26\%(\tfrac{3}{2},\tfrac{3}{2})$
		144.114	0.0001	$0 \to 1$	$83\%(^2D)^3D, 17\%(^2D)^3P$	$74\%(\tfrac{3}{2},\tfrac{3}{2}), 26\%(\tfrac{3}{2},\tfrac{1}{2})$
$3d^94s^24p^66p$		149.370	0.0048	$0 \to 1$	$57\%(^2D)^1P, 31\%(^2D)^3P, \underline{10\%}(^2D)^3D$	$98\%(\tfrac{5}{2},\tfrac{3}{2}), 2\%(\tfrac{5}{2},\tfrac{7}{2})$
$3d^94s^24p^64f$	149.83	149.387	0.0028	$0 \to 1$	$79\%(^2D)^3P, \underline{13\%}(^2D)^1P, \underline{7\%}(^2D)^3D$	$56\%(\tfrac{5}{2},\tfrac{7}{2}), \underline{43\%}(\tfrac{5}{2},\tfrac{7}{2}), 1\%(\tfrac{5}{2},\tfrac{3}{2})$
$3d^94s^24p^64f$		149.400	0.0075	$0 \to 1$	$53\%(^2D)^3D, \underline{46\%}(^2D)^1P$	$\underline{56\%}(\tfrac{5}{2},\tfrac{7}{2}), \underline{44\%}(\tfrac{5}{2},\tfrac{5}{2}), 1\%(\tfrac{5}{2},\tfrac{3}{2})$
$3d^94s^24p^66p$		151.048	0.0043	$0 \to 1$	$50\%(^2D)^3P, \underline{41\%}(^2D)^1P, \underline{9\%}(^2D)^2D$	$\underline{75\%}(\tfrac{3}{2},\tfrac{1}{2}), 25\%(\tfrac{3}{2},\tfrac{3}{2})$
$3d^94s^24p^66p$	151.61	151.104	0.0000	$0 \to 1$	$82\%(^2D)^3D, 18\%(^2D)^3P$	$75\%(\tfrac{3}{2},\tfrac{3}{2}), 25\%(\tfrac{3}{2},\tfrac{1}{2})$
$3d^94s^24p^64f$		151.130	0.0060	$0 \to 1$	$40\%(^2D)^3D, 40\%(^3D)^1P, 20\%(^2D)^3P$	$100\%(\tfrac{3}{2},\tfrac{5}{2})$
$3d^94s^24p^65f$		152.282	0.0012	$0 \to 1$	$80\%(^2D)^3P, \underline{10\%}(^2D)^3D, \underline{10\%}(^2D)^1P$	$64\%(\tfrac{5}{2},\tfrac{5}{2}), \underline{36\%}(\tfrac{5}{2},\tfrac{7}{2})$
$3d^94s^24p^65f$	152.78	152.290	0.0059	$0 \to 1$	$50\%(^2D)^3D, \underline{50\%}(^2D)^1P$	$\underline{64\%}(\tfrac{5}{2},\tfrac{7}{2}), \underline{36\%}(\tfrac{5}{2},\tfrac{5}{2})$
$3d^94s^24p^67p$		152.342	0.0038	$0 \to 1$	$59\%(^2D)^1P, 31\%(^2D)^3P, \underline{10\%}(^2D)^3D$	$100\%(\tfrac{5}{2},\tfrac{3}{2})$
$3d^94s^24p^66f$		153.856	0.0006	$0 \to 1$	$80\%(^2D)^3P, \underline{12\%}(^2D)^3D, \underline{8\%}(^2D)^1P$	$68\%(\tfrac{5}{2},\tfrac{5}{2}), \underline{32\%}(\tfrac{5}{2},\tfrac{7}{2})$
$3d^94s^24p^66f$		153.862	0.0045	$0 \to 1$	$52\%(^2D)^1P, \underline{48\%}(^2D)^3D$	$68\%(\tfrac{5}{2},\tfrac{7}{2}), 32\%(\tfrac{5}{2},\tfrac{5}{2})$
$3d^94s^24p^68p$	154.38	153.911	0.0017	$0 \to 1$	$59\%(^2D)^1P, 31\%(^2D)^3P, \underline{10\%}(^3D)^3D$	$100\%(\tfrac{5}{2},\tfrac{3}{2})$
$3d^94s^24p^65f$		154.022	0.0047	$0 \to 1$	$40\%(^2D)^3D, 40\%(^2D)^1P, 20\%(^2D)^3P$	$100\%(\tfrac{3}{2},\tfrac{5}{2})$
$3d^94s^24p^{56}7p$		154.048	0.0032	$0 \to 1$	$48\%(^2D)^3P, \underline{40\%}(^2D)^1P, \underline{10\%}(^2D)^3D$	$\underline{77\%}(\tfrac{3}{2},\tfrac{1}{2}), 22\%(\tfrac{3}{2},\tfrac{3}{2})$
$3d^94s^24p^67p$		154.075	0.0000	$0 \to 1$	$80\%(^2D)^3D, 20\%(^2D)^3P$	$77\%(\tfrac{3}{2},\tfrac{3}{2}), 22\%(\tfrac{3}{2},\tfrac{1}{2})$
$3d^94s^24p^66f$		155.595	0.0035	$0 \to 1$	$40\%(^2D)^1P, 40\%(^2D)^3D, 20\%(^2D)^3P$	$100\%(\tfrac{3}{2},\tfrac{5}{2})$
$3d^94s^24p^68p$	156.15	155.629	0.0014	$0 \to 1$	$50\%(^2D)^3P, \underline{40\%}(^2D)^1P, \underline{10\%}(^2D)^3D$	$\underline{77\%}(\tfrac{3}{2},\tfrac{1}{2}), 23\%(\tfrac{3}{2},\tfrac{3}{2})$
$3d^94s^24p^68p$		155.645	0.0000	$0 \to 1$	$80\%(^2D)^3D, 19\%(^2D)^3P$	$77\%(\tfrac{3}{2},\tfrac{3}{2}), 23\%(\tfrac{3}{2},\tfrac{1}{2})$

perimental spectrum. These percentages correspond to a Boltzmann distribution among the levels of a 1-eV plasma which is consistent with the CR model predictions and also gives the optimum agreement with the experimental profiles. According to the CR model the initial plasma electron temperature was approximately 3.3 eV; in practice the effects of the decrease in plasma temperature with expansion will be somewhat compensated for by the increased lifetime of the $3d^94d$ levels because of the reduced collisional decay rate at lower temperature and density. So after 82 ns the average electron temperature will be somewhat lower than 1 eV. The closeness of
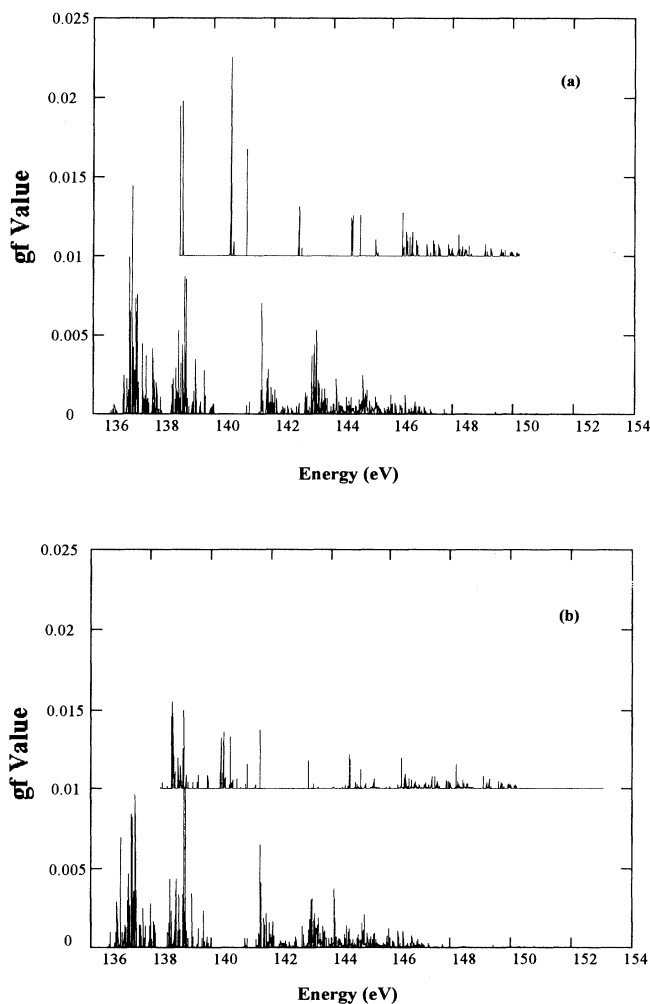
FIG. 4. This shows the effects of including configuration interaction in the calculation of the $3d$ absorption spectrum of Sr II. Part (a) shows stick plots of the spectra Sr II $3d^{10}4s^24p^65s$ $\rightarrow 3d^94s^24p^65s[np,mf]$, and Sr II $3d^{10}4s^24p^64d$ $\rightarrow 3d^94s^24p^64d[np,mf]$ one above the other, calculated without configuration interaction effects in the excited state. Part (b) shows stick plots of the spectra Sr II $3d^{10}4s^24p^65s$ $\rightarrow 3d^94s^24p^6[5s+4d][np,mf]$, and Sr II $3d^{10}4s^24p^64d$ $\rightarrow 3d^94s^24p^6[4d+5s][np,mf]$ one above the other, calculated with configuration-interaction effects included in the excited states. In all of the above n ranged from 5 to 11 and m ranged from 4 to 9.

the fit between theoretical prediction and experiment facilitated the classification of the observed features, which are labeled according to their strongest component transitions in Table II. It should be noted that the excited-state basis consisted of over 1000 terms, and the total number of possible transitions linking these to the $3d^{10}5s$ and $3d^{10}4d$ states is 3038, so in preparing Table II only lines with a gf value in excess of 0.0019 were considered. Comparison of eigenvector purities in different coupling schemes showed the average purity to be 36% in LS compared to 50% in jj. However, the LS scheme was used to designate the levels for ease of presentation. Moreover, from Table II it is evident that configuration-interaction (CI) effects are extremely important especially between $3d^95snl$ and $3d^94dnl$ configurations. To explore the effects of this interaction on the spectrum, further HXR calculations were performed for $3d^{10}5s \rightarrow 3d^95snl$ and $3d^{10}4d \rightarrow 3d^94dnl$ transitions in which there was no allowance for upper state mixing. The results of these calculations are presented in Fig. 4, where they are com-
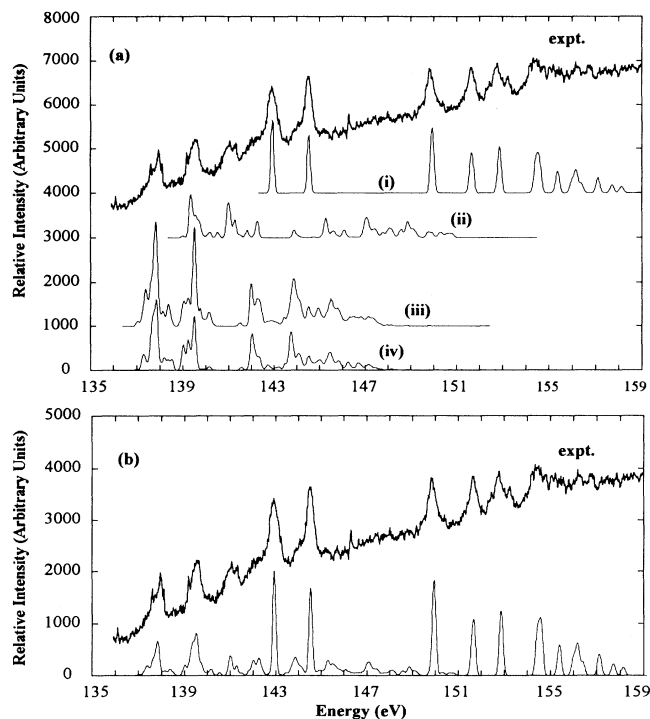

FIG. 5. Plot of the microdensitometer trace of a strontium laser-produced plasma of column length 2 mm taken at an interplasma time delay of 63 ns. Part (a) shows the trace and the theoretical spectra (i) Sr III $3d^{10}4s^24p^6 \rightarrow 3d^94s^24p^6[np,mf]$, (ii) Sr II $3d^{10}4s^24p^65s \rightarrow 3d^94s^24p^6[5s+4d][np,mf]$, (iii) Sr II $3d^{10}4s^24p^64d(j=\frac{5}{2}) \rightarrow 3d^94s^24p^6[4d+5s][np,mf]$, and (iv) Sr II $3d^{10}4s^24p^64d(j=\frac{3}{2}) \rightarrow 3d^94s^24p^6[4d+5s][np,mf]$, which were shifted by the following amounts +0.55, +0.65, +0.4, and +0.4 eV, respectively, to fit the observed data. In all of the above n ranged from 5 to 11 and m ranged from 4 to 9. Part (b) shows these spectra combined into the one plot in the ratios 60:24:10:6, respectively, and compared with the observed absorption. All of the spectral lines in the theoretical plots have been given a Gaussian width of 0.1 eV.

C. McGUINNESS *et al.*

pared with the previous data. There are noticeable differences, especially in intensities which would lead to a very different spectral profile in Fig. 3 if CI effects were excluded. Finally it is instructive to reconsider the spectrum recorded at $\tau = 197$ ns (Fig. 2). Here the effects of excited-state absorption are significantly reduced, and indeed the best fit is obtained with an initial population of $70\% 3d^{10}5s + 30\% 3d^{10}4d$ which is consistent with $T_e = 0.5$ eV [Fig. 2(b)].

THE 3d SPECTRUM OF Sr²⁺

In Sr²⁺ the lack of an occupied 5s subshell simplifies the situation in a number of important ways. First, there are no line splittings due to interactions with 5s electrons; second $(4d + 5s)$ mixing does not occur; and finally, there are no metastable levels just about the ground state. The 3d spectrum of Sr²⁺ is presented in Fig. 5, where the features form what appears to be a simple Rydberg series. They are weakly evident in the 82-ns spectrum, but dominate the $\tau = 60$-ns spectrum. Some internal structure is clearly evident in the higher-energy lines. Detailed
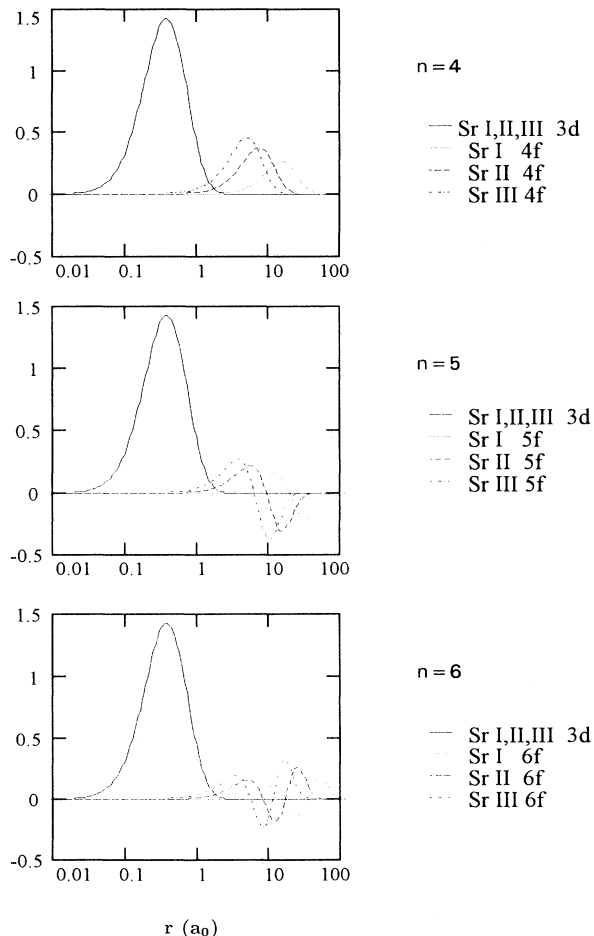
FIG. 6. Radial wave-function plots of the 3d wave function and nf wave functions $(n = 4-6)$ for Sr I, Sr II, and Sr III, respectively.
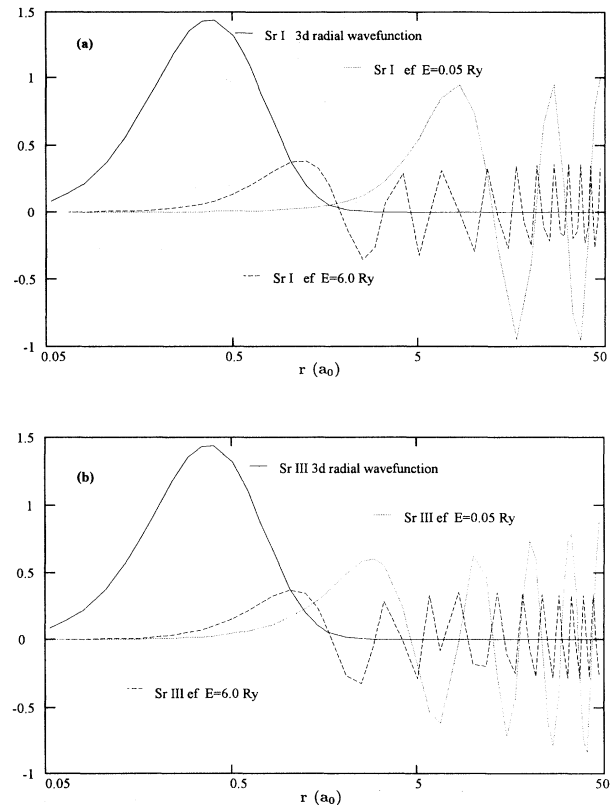

FIG. 7. Radial wave-function plots of the 3d wave function and two εf wave functions of differing energies $(E = 0.05$ and 6.0 Ry, respectively) (a) in Sr I, (b) in Sr III.

configuration-interaction calculations for $3d^{10}4s^24p^6 \rightarrow 3d^94s^24p^6(nf + mp)$ transitions $(4 \leq n \leq 10, 5 \leq m \leq 10)$ show that, apart from the first two lines which arise from $3d^{10} \rightarrow 3d^95p$ excitation, the features, are in fact composed of overlapping $3d \rightarrow mp$ and $3d \rightarrow nf$ transitions which combine in such a way that only a few strong lines, corresponding to those observed, are predicted to appear.
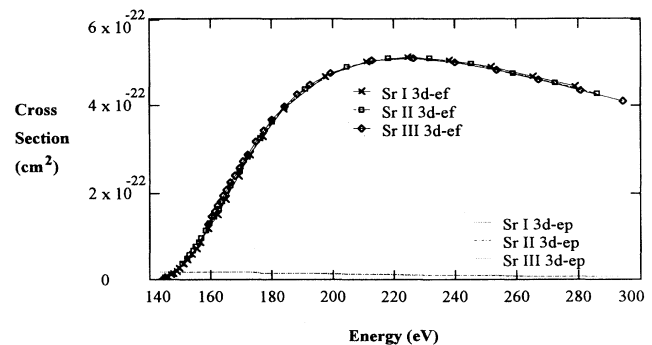

FIG. 8. Plot of the calculated photoionization cross section of the 3d orbital for the ion stages Sr I, Sr II, and Sr III. Note that the $3d$-εf photoionization cross section shows a maximum above threshold in all ion stages, whereas the $3d$-εp photoionization cross section of all the ion stages is substantially smaller and decreases monotonically above threshold.

TABLE IV. The 3d photoabsorption spectrum of Sr IV. Lower level: $3d^{10}4s^24p^5$.

Upper level:	λ (Å) Expt.	Calc.	gf value:	$J \rightarrow J$	LS composition:	jj composition
$3d^94s^24p^6$	115.08	114.620	0.2828	$\frac{3}{2} \rightarrow \frac{5}{2}$	100% ^2D	100% ($\frac{5}{2}$)
	115.64	115.208	0.1579	$\frac{1}{2} \rightarrow \frac{3}{2}$	100% ^2D	100% ($\frac{3}{2}$)
	116.76	116.354	0.0319	$\frac{3}{2} \rightarrow \frac{3}{2}$	100% ^2D	100% ($\frac{3}{2}$

These predicted lines are also shown in Fig. 5. Note that in producing this figure the theoretical data were shifted systematically by 0.55 eV to give the best agreement between calculation and observation. As in Fig. 2(a) a ratio Sr^{2+} to Sr^+ of $\frac{3}{2}$ was used to weight the theoretical spectrum for the purpose of comparison, as both Sr^{2+} and Sr^+ are present in the experimental spectrum. The classifications are presented in Table III from which it is seen that $3d^9nf$ and $3d^9mp$ configurations up to $n = 6$ and $m = 8$ contribute to the features observed here. At higher n and m the series weaken and merge in such a way that it was not possible to locate any further discrete structure. The increase in intensity of the $3d$-nf transitions relative to Sr and Sr^+ is due to nf contraction due to the increased Coulomb attraction of the core. In Fig. 6, comparison is made between $3d$, $4f$, and $5f$ radial wave functions for Sr, Sr^+, and Sr^{2+}. The increased $3d, nf$ overlap leads to an increase in oscillator strength. However, unlike the case of $3d$ collapse in the Ar I sequence [25] or $4f$ collapse in the Xe I sequence [26,27], there is effectively no hybridization between different nf states and no term dependence. The latter is usually found for cases where the total potential has two minima at large and small values of r, and the excited wave function penetrates the centrifugal barrier and has a finite amplitude in the inner well and the spectrum contains a strong $nl \rightarrow n, \varepsilon l + 1$ resonance near threshold. In the present case the potential has no inner well, and the $3d$-εf cross section is expected to contain a delayed onset near threshold in line with earlier predictions for Ar I and observation of Sr I [28,29].

To see if the cross section is altered with increasing ionization, continuum εf and εp wave functions were calculated from the HXR code. The increased core penetration due to increasing ionization is immediately obvious

from Fig. 7. Using these radial wave functions the $\langle 3d|r|\varepsilon l\rangle$ matrix elements were evaluated and then the formula of Manson and Cooper [28] applied to calculate the $3d \rightarrow \varepsilon p, \varepsilon f$ cross sections. The results of these calculations are shown in Fig. 8. The $3d \rightarrow \varepsilon p$ cross section decays hydrogenically, while the $3d \rightarrow \varepsilon f$ exhibits a Cooper minimum at threshold. The energy of this minimum does not change between Sr and Sr^{2+}. The increased penetration of the εf wave function into the $3d$ region and the consequent change in $\langle 3d|r\varepsilon f\rangle$ causes the $3d \rightarrow \varepsilon f$ cross section to peak closer to threshold with increasing ionization. However, at the same time the $3d$ ionization energy is increasing so that the cross section as a function of energy is effectively unaltered. The peak in the Sr I cross section at 220 eV is 30 eV higher than the value reported in the earlier published data [29]. In the present case it was not possible to extract continuum absorption profiles from densitometer traces as the background continuum was strongly modulated at these energies.

Finally it should be noted that three features observed in the shortest τ spectrum between 115 and 117 eV can be identified as $3d^{10}4s^24p^5 - 3d^94s^24p^6$ transitions in Sr^{3+} (Table IV).

ACKNOWLEDGMENTS

[1] M. W. D. Mansfield and J. P. Connerade, Proc. R. Soc. London Ser. A 342, 421 (1975).

[2] M. W. D. Mansfield and G. H. Newsom, Proc. R. London Ser. A 377, 431 (1981).

[3] M. W. D. Mansfield and J. P. Connerade, J. Phys. B 15, 503 (1982).

[4] N. Martinsson and B. Johansson, J. Phys. B 14, L37 (1981).

[5] D. M. P. Holland and K. Codling, J. Phys. B 14, 2345 (1981).

[6] T. Nagata, J. B. West, T. Hayashi, Y. Itikawa, Y. Itoh, T. Koizumi, J. Murakami, Y. Sato, H. Shibata, A. Yagishita, and M. Yoshino, J. Phys. B 19, 1281 (1986).

[7] I. C. Lyon, B. Peart, and K. Dolder, J. Phys. B 20, 1925 (1987).

[8] B. Peart and K. Dolder, J. Phys. B 8, 56 (1975).

[9] J. T. Costello, W. G. Lynam, and P. K. Carroll, J. Phys. (Paris) Colloq. 49, C1-243 (1988).

[10] J. M. Bizeau, D. Cubaynes, M. Richter, F. J. Wuilleumier, J. Obert, J. C. Puteux, T. J. Morgan, E. Källne, S. Sorensen, and A. Damanay, Phys. Rev. Lett. 67, 576 (1991).

[11] V. K. Ivanov and J. B. West, J. Phys. B 26, 2099 (1993).

[12] J. T. Costello, E. T. Kennedy, J. P. Mosnier, P. K. Carroll, and G. O'Sullivan, Phys. Scr. T 34, 77 (1991).

[13] P. Dunne, G. O'Sullivan, and V. K. Ivanov, Phys. Rev. A

48, 4358 (1993).

[14] J. T. Costello, D. Evans, R. B. Hopkins, E. T. Kennedy, L. Kiernan, M. W. D. Mansfield, P. Mosnier, M. H. Sayeed, and B. F. Sonntag, J. Phys. B **25**, 5055 (1992).

[15] J. T. Costello, E. T. Kennedy, B. F. Sonntag, and C. L. Cromer, J. Phys. B **24**, 5063 (1991).

[16] J. E. Hansen, J. Brilly, E. T. Kennedy, and G. O'Sullivan, Phys. Rev. Lett. **63**, 1934 (1989).

[17] P. K. Carroll, E. T. Kennedy, and G. O'Sullivan, Appl. Opt. **19**, 1454 (1980).

[18] D. F. Colombant and G. F. Tonon, J. Appl. Phys. **44**, 3524 (1973).

[19] R. L. Kelly, O.R.N.L. Report No. 5922 (1982) (unpublished).

[20] R. D. Cowan, *The Theory of Atomic Structure and Spectra* (University of California Press, Berkeley, 1981).

[21] E. J. McGuire, Phys. Rev. A **5**, 1043 (1972).

[22] H. Aksela, S. Aksela, R. Lakanen, J. Tulkki, and T. Åberg, Phys. Rev. A **42**, 5192 (1990).

[23] T. Koizumi, T. Hayaishi, Y. Itakawa, T. Nagata, Y. Sato, and A. Yagishita, J. Phys. B **20**, 5393 (1987).

[24] C. E. Moore, Atomic Energy Levels Vol. II Natl. Bur. Standards Circ. 467. U.S. Government Printing Office, Washington, D.C. (1958).

[25] R. D. Cowan, J. Opt. Soc. Am. **58**, 924 (1968).

[26] T. B. Lucatorto, T. J. McIlrath, J. Sugar, and S. M. Younger, Phys. Rev. Lett. **47**, 1124 (1981).

[27] J. P. Connerade and M. W. D. Mansfield, Phys. Rev. Lett. **48**, 131 (1982).

[28] S. T. Manson and J. W. Cooper, Phys. Rev. **165**, 126 (1968).

[29] J. P. Connerade and M. W. D. Mansfield, Proc. R. Soc. London Ser. A **352**, 557 (1977).